IOP Publishing Journal of Micromechanics and Microengineering
J. Micromech. Microeng. **24** (2014) 065011 (10pp) doi:10.1088/0960-1317/24/6/065011

iGC2: an architecture for micro gas chromatographs utilizing integrated bi-directional pumps and multi-stage preconcentrators

Yutao Qin and Yogesh B Gianchandani

Center for Wireless Integrated MicroSensing and Systems (WIMS^2), University of Michigan, Ann Arbor, MI 48109, USA

E-mail: yutaoqin@umich.edu and yogesh@umich.edu

Received 17 December 2013, revised 27 February 2014
Accepted for publication 3 April 2014
Published 6 May 2014

Abstract

This paper reports an integrated micro gas chromatography (μGC) architecture which utilizes a bi-directional micropump. Four integral components—the bi-directional Knudsen pump (KP2), a two-stage preconcentrator-focuser (PCF2), a separation column, and a gas detector—are integrated in a 4.3 cm^3 stack, forming a serial flow path. All four components are fabricated using the same three-mask process. Compared to the conventional approach used with multi-stage preconcentrators, in which valves are used to reverse flow between the sampling phase and the separation phase, this μGC architecture reduces the overall complexity. In this architecture, the vapors being sampled are drawn through the detector and column before reaching the PCF2. The microsystem operation is experimentally validated by quantitative analyses of benzene, toluene, and xylene vapors ranging in concentration from 43–1167 mg m^{-3}.

Keywords: quantitative analysis, BTX sensor, Knudsen pump, thermal transpiration, microdischarge

(Some figures may appear in colour only in the online journal)

1. Introduction

Following the pioneering work of Terry *et al* [1], a variety of micro gas chromatography (μGC) systems have been reported over the past three decades. Many μGC systems include microfabricated renditions of three components that are integral to the system: the preconcentrator, which samples vapor analytes and provides vapor injection; the column, which separates the vapor analytes; and the gas detector, which quantifies the eluents from the column [2–5]. These systems use external, commercial pumps to provide gas flow. More recent systems utilizing micropumps have also been demonstrated [6–8]. Some systems use commercial valves to control fluidic routing; microfabricated valves for μGC systems are being studied [4].

In the simplest architectures, the preconcentrator, column, detector, and pump are connected in series, and operated with unidirectional flow from the preconcentrator to the column and then the detector [2, 8]. In others, a valve bypasses the column during vapor sampling to increase the flow rate, but the flow direction in both sampling and analytical separation remains the same [4, 9]. The bypass-flow architecture can be further enhanced by using an additional detector in the bypass line, which provides a coarse measurement of the vapor concentration and informs the system of the optimal sampling time [9]. In more complex architectures, a number of valves are used to reverse the flow direction in the preconcentrator during sampling and separation (i.e., bi-directional flow is necessary) [10–12]. As a consequence, during the sampling phase vapors enter the preconcentrator at the end which will be downstream during the analytical separation phase.

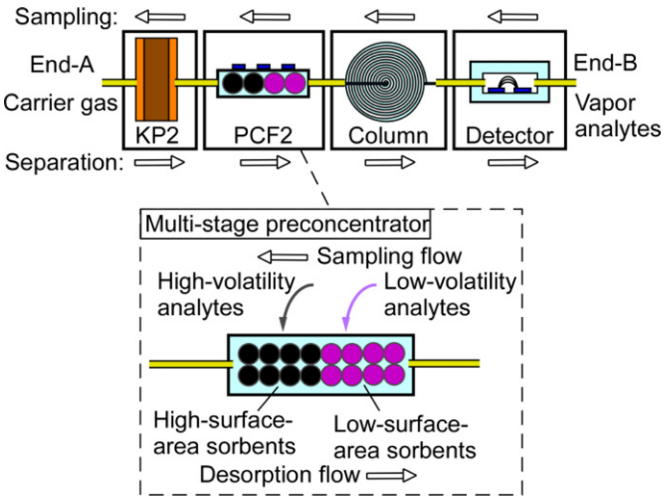

Figure 1. Bi-directional operation of the *iGC2* system. During vapor sampling, the KP2 draws vapor analytes through the detector and column, and into the PCF2. The two stages of PCF2 target analytes with different volatility ranges. The flow is reversed during analytical separation.

While bi-directional flow is potentially beneficial for a single-stage preconcentrator, it is essential for a multi-stage (or multi-bed) one. A multi-stage preconcentrator uses various types of sorbents for analyses of vapor analytes of broad ranges of volatilities. The stages, each packed with one type of sorbent, are connected in series. During the vapor sampling phase, analytes with low volatility are trapped in stages that are upstream in the sampling flow path; these stages are packed with sorbents of low surface area. Analytes with high volatility, after passing through the upstream stages, are trapped in downstream stages, which are packed with sorbents of high surface area (figure 1). During the analytical separation phase, the flow direction is reversed, allowing all the trapped analytes to be injected into the separation column [13].

Miniaturization of valves has been a subject of extensive research [14]. Many of the microvalves reported to date utilize the actuation of a flexible diaphragm to control flow. This actuation has been performed electrostatically [15], piezoelectrically [16], or thermopneumatically [17]. A microvalve targeting μGC integration has been reported [18]. However, the use of a deformable diaphragm introduces additional cost, complexity, and reliability challenges to a multi-component μGC system that is already complex. This paper evaluates a valveless μGC architecture, the *iGC2*, which is comprised of a bi-directional Knudsen pump (KP2), a two-stage preconcentrator (PCF2), a separation column, and a detector[1]. Its operation is illustrated in figure 1. During the sampling phase, vapor analytes enter the system, pass through the detector and column, and finally settle into the PCF2. During the analytical separation phase, the flow direction is reversed by the KP2; the sampled vapor analytes are then thermally desorbed from the PCF2, separated in the column, and quantified by the detector.

Valveless bi-directional operation is more amenable to μGC systems than to conventional benchtop GC systems. In

[1] Portions of this paper appear in conference abstract form in [19].

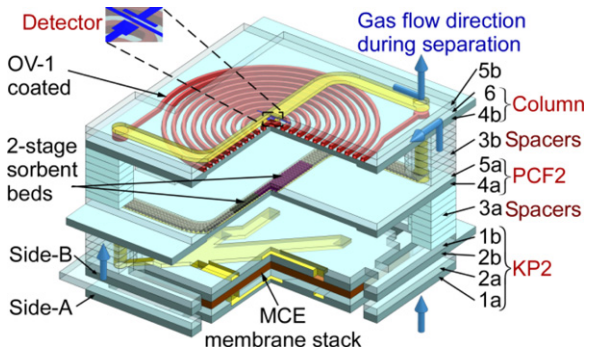

Figure 2. Structural concept of the *iGC2* system. The KP2, PCF2, column, and detector are stack integrated. Spacers are used to provide inter-layer flow connection.

contrast to conventional columns, which are usually 10–30 m long, microcolumns typically have relatively small lengths of 0.08–3 m [4, 20, 21]. Qualitatively, the short microcolumns have small 'breakthrough' volumes, i.e., vapors can easily pass through the column and reach the preconcentrator during sampling. At the end of the sampling period, residual vapors may remain in the column. When flow is reversed to initiate the separation phase, the vapors in the column are purged, but may contribute to a baseline response upon which the retention peaks are superposed. By accommodating these trends into the quantitative assessment of retention peaks, quantitative analyses are not compromised.

The design of the *iGC2* system is described in section 2; fabrication is described in section 3; experimental results are presented in section 4, followed by the discussion and conclusion in section 5.

2. Design

2.1. Bi-directional Knudsen pump (KP2)

Knudsen pumps are motionless gas pumps that operate on the principle of thermal transpiration [22, 23]. One type of Knudsen pump implementation utilizes nanoporous mixed cellulose ester (MCE) membrane(s) (of thickness ≈105 μm, pore diameter ≈25 nm, porosity ≈70%, Millipore, MA) [24]. In the presence of a temperature gradient, flow is generated from the cold side to the hot side of the MCE membrane(s). A previously reported bi-directional Knudsen pump used thermoelectric elements to apply reversible temperature gradients across the MCE membrane(s) [25]. In the *iGC2* architecture, however, the KP2 simply utilizes thin-film Joule heaters on both sides of a membrane stack. During operation, one of the sides is heated while the other is cooled passively (by a heat sink or natural convection).

The KP2 has a stack of four MCE membranes sandwiched by two glass dice on each side, i.e., Side-A and Side-B, (figure 2). Each glass die is ≈500 μm thick. On Side-A, the glass die that is in contact with the MCE membrane stack (i.e., Die 2a) has a thin-film metal heater and thermistor to control the temperature, as well as multiple through-holes to facilitate gas flow into and out of the MCE membranes. The other glass die (i.e., Die 1a) has in-plane grooves that guide gas streams to a single port, which can be connected to other components

or an external test setup. The constituent glass dice on Side-B (i.e., Die 1b and Die 2b) are identical to Die 1a and Die 2a, respectively.

In the *iGC2* stack assembly (figure 2), Side-B is attached to the rest of the stack, whereas Side-A is attached to an external heat sink. During analytical separation, Side-B is heated while Side-A is cooled by the heat sink. During vapor sampling, Side-A (and the heat sink) is heated while Side-B is cooled by natural convection together with the rest of the stack.

2.2. Two-stage preconcentrator (PCF2)

Previously reported microfabricated multi-stage preconcentrators used multiple chambers, each containing one type of sorbent [10, 13]. In the *iGC2*, however, the PCF2 contains only one chamber designed in the shape of a channel; the two stages are formed by packing different sorbents in sequence. This design mimics its macro-scale counterpart: the multi-bed thermal desorption tube. It can be configured to include more than two stages without redesign.

The PCF2 consists of a channel (width ≈1 mm, depth ≈200 μm) formed by Die 4a and Die 5a (figure 2). The channel is packed with four segments of particles in series: glass beads (with diameter 150–180 μm, Sigma Aldrich, WI); Carbograph 2 (with surface area ≈10 $m^2\ g^{-1}$, diameter 120–150 μm, Grace Davison Discovery Sciences, IL); Carbopack B (with surface area ≈100 $m^2\ g^{-1}$, diameter 112–140 μm, Sigma Aldrich, WI); glass beads (with diameter 150–180 μm, Sigma Aldrich, WI). The segment of Carbograph 2 is intended to trap vapors of lower volatility (e.g., toluene and xylene), and the segment of Carbopack B is intended to trap vapors of higher volatility (e.g., benzene). The two segments of glass beads, one at each end of the PCF2 channel, are used to confine the two segments of sorbents in the central region of the device, where the temperature is the highest during thermal desorption.

The PCF2 has advantages over our prior preconcentrator design [8] because its narrower channel dimension provides less sensitivity to the non-uniformity of sorbent packing, as well as higher flow velocity at a given volumetric flow rate. A future design can be improved, presumably, by incorporating the pillar structures and sorbent loading port [8, 26].

2.3. Column, detector, and the stacked iGC2 system

The *iGC2* separation column is a channel (of length ≈25 cm and hydraulic diameter ≈230 μm) coated with a layer of ≈0.2 μm thick non-polar polydimethylsiloxane (PDMS or OV-1, Ohio Valley Specialty, OH) that serves as the stationary phase [8]. The column is formed by Die 4b and Die 6 (figure 2). When passing along the separation column, vapor mixtures partition between the stationary phase material and the carrier gas. The non-polar PDMS stationary phase used in this work interacts with the vapor molecules mainly by van der Waals force [27]. Vapor molecules with higher molecular weight typically have a stronger interaction with the stationary phase and display a longer retention time. Additionally, thicker coatings of the stationary phase provide a stronger interaction with the vapor molecules and extend retention times.

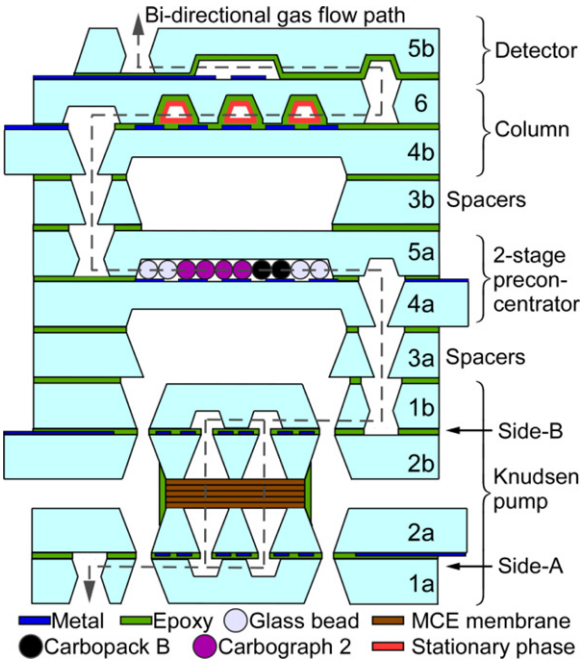

Figure 3. Illustration of the cross-section of the *iGC2* system. The four components—pump, preconcentrator, separation column, and detector—form a serial gas flow path, as indicated by the gray dashed line.

The gas detector consists of two thin-film metal electrodes on a glass substrate (i.e., Die 6). In this work, the metal layer consists of Ti/Pt of thickness 25/100 nm. The two electrodes (i.e., anode and cathode) are spaced 50–200 μm apart. Electrodes of other materials, thickness, and separation can also be used. The groove in Die 5b forms the detector channel that guides gas flow over the electrodes (figure 2). By applying a voltage pulse between the two electrodes, a microdischarge is generated. The resulting optical intensity at the line that is specific to the C–H emission can be used to quantify carbon-containing species in the gas flow [8, 28]. In contrast to the flame ionization detectors (FID) that are often used within commercial GC systems, microdischarge-based detectors do not require a stored supply of H_2 to create the ionization, and are more amenable to monolithic integration.

The KP2, PCF2, column, and detector are integrated in the form of a stack (figures 2 and 3), which also uses fourteen 500 μm thick glass spacers (Dice 3a and Dice 3b). The spacers provide thermal isolation between adjacent components. Perforations in the spacers allow inter-layer flow. The dashed line in figure 3 indicates the gas flow path of the system.

3. Fabrication

The constitutive elements of all four *iGC2* components, as well as the spacers, are fabricated on glass wafers using the same three-mask lithographic processes. Hence, these elements may be either fabricated on separate wafers or all on a single wafer. The use of glass as the substrate material has several benefits. It is lower in cost than silicon and ceramic options, and can be easily micromachined. In addition, the transparent nature of

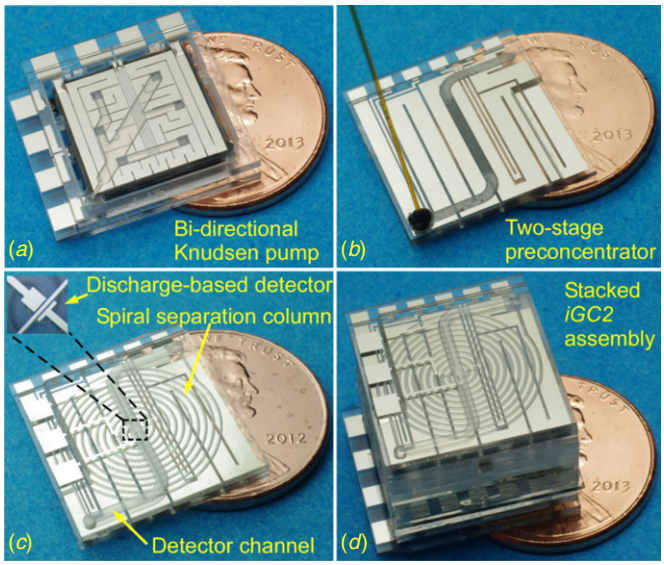

Figure 4. Photographs of the *iGC2* system. (*a*) The KP2, (*b*) the PCF2, (*c*) the separation column and the discharge-based detector, and (*d*) the *iGC2* system, which has a footprint of 2 × 1.8 cm^2 and a volume of 4.3 cm^3.

glass permits visual inspection of the interior of the devices, which benefits early stage research and development.

First, a Ti/Pt thin film (of thickness 25/100 nm) is deposited and patterned to form heaters, thermistors, and discharge electrodes (using Mask #1). The glass wafer is micromachined on both sides by sandblasting (Bullen, Inc., OH) to create fluidic channels and thermal-isolating cutouts (using Mask #2–3).

After wafer dicing, the glass dice are assembled together. The constituent dice of the separation column are spin-coated with an SU-8 (MicroChem, MA) layer, which, smoothens the sandblasted surface and also serves as an adhesive between dice. The column is also coated with the OV-1 stationary phase using a static coating method, in which an OV-1/pentane solution is first filled into the column and subsequently the pentane is evaporated under vacuum [29]. The resulting thickness of the stationary phase is expected to be in the range of 0.2 μm. The other dice are held in place by a low-viscosity epoxy (Model # Epotek 377, Epoxy Technology, Inc., MA). The MCE membrane stack of the KP2 is sealed around the perimeter by a viscous epoxy (Model # Stycast2850FT, Henkel, Germany).

The PCF2 is packed with sorbent particles. In this preliminary PCF2 design, which does not have embedded features for confining the sorbent particles, a small segment of capillary tube (with inner diameter ≈100 μm, length ≈2 mm) is attached to one end of the channel. With a gentle vacuum applied at this end, the sorbent particles and glass beads are drawn into the PCF2 channel [26], in sequence, from the other end, which is later attached to another similar segment of capillary tube.

The four components and the spacers are finally integrated into a stack. Adhesion between the components and spacers is provided by either an epoxy or a wax bond layer. Photographs of the fabricated components and system are shown in figure 4.

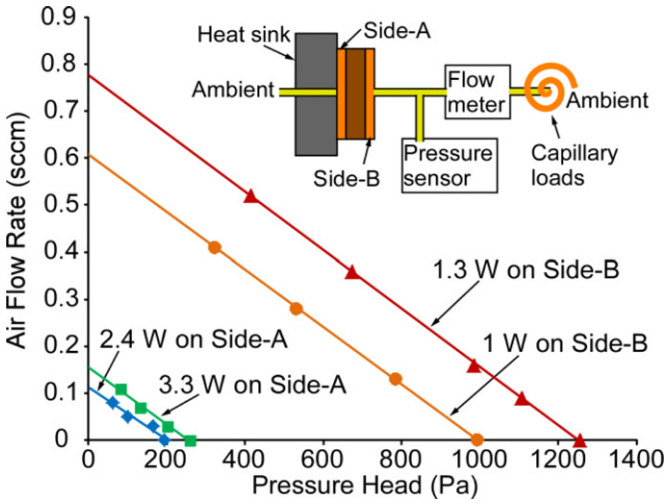

Figure 5. The test setup and steady state performance of the KP2. The data points were obtained by altering the capillary loads and were linearly fitted to indicate the characteristic lines of the KP2.

The *iGC2* system has a footprint of 1.8 × 2.0 cm^2 and a volume of 4.3 cm^3.

4. Experimental results

In order to characterize their performance, the KP2 and PCF2 were separately evaluated without assembly into the full *iGC2* system. The experimental evaluations focused on the aromatic hydrocarbons benzene, toluene, and *m*-xylene (BTX), which are typical indoor pollutants.

4.1. KP2

The KP2 was evaluated by measuring its pressure-flow characteristics. As indicated in section 2, Side-A of the KP2 was attached to an aluminum block that served as a heat sink. In the evaluation of the standalone pumps, Side-B was not attached to the other *iGC2* components. As shown in figure 5, a commercial pressure sensor (Model # MPX5010DP, Freescale Semiconductor, AZ) and a flow meter (Part # FMA-1603A, Omega Engineering, CT) were used to monitor the pressure head and flow, respectively. Although the former had a rated maximum error of ±500 Pa (including offset variation), the actual error was expected to be much smaller, because it was used at room temperature within a small pressure range and corrected for offset. The latter had a rated error of ±0.02 sccm. Varying flow loads (manifested as capillary tubes with varying lengths and inner diameters) were used to obtain various pressure-flow points. The values of the loads were selected to span a wide range covering the actual load provided by the rest of the *iGC2* system.

With 1.3 W power applied on Side-B, the pumps typically provided a steady state air flow rate of 0.52 sccm for a pressure head of 413 Pa; the blocking pressure head, at which the flow was reduced to zero, was 1254 Pa. This direction of flow is intended for the analytical separation. In the opposite direction, with 3.3 W power applied on Side-A (with the heat sink still in place, and Side-B cooled only by natural convection), the

pump provided a steady state air flow rate of 0.11 sccm against a pressure head of 87 Pa; the blocking pressure was 259 Pa (figure 5). In general, the relationship between the input power of the KP2 and the flow rate are approximately linear for intermediate pressure heads.

4.2. PCF2

The PCF2 was characterized for both adsorption and desorption of BTX. The adsorption capability of preconcentrators is often characterized by the time taken for the vapor analytes flowing through the component to saturate the concentration measured at the exit; this is known as 'breakthrough' [13]. For the PCF2, the inlet (for vapor sampling) was connected to a 2 L dilution bottle (Sigma Aldrich, WI) containing the vapor of benzene, toluene, or *m*-xylene in N_2. The component BTX vapors were individually drawn by a vacuum pump through the PCF2 at flow rates of 0.1, 0.3, and 0.4 sccm. A fixed volume (100 μL) of vapor exiting the PCF2 was periodically routed by a six-port valve to an FID within a commercial GC (Model # Agilent 6890).

In figure 6(*a*), the BTX concentrations at the preconcentrator outlet c_{out} are normalized to that at its inlet c_{in}; the vapor sampling volume is calculated as the product of sampling flow rate and sampling time. Conventionally, the breakthrough criterion is selected at the point when c_{out}/c_{in} reaches 10% [13]. Using this criterion, the PCF2 in this effort had breakthrough volumes of 0.5, 5.4, and 17.6 cm^3 for benzene, toluene, and *m*-xylene, respectively.

The thermal desorption characteristics of the PCF2 were evaluated by the desorption peaks observed in chromatograms. The PCF2 was first used to sample an individual analyte vapor (i.e., benzene, or toluene, or *m*-xylene) at 0.1 sccm for 10 min. Then it was connected upstream of the FID and downstream of an injection port in a commercial GC (Agilent 6890), which provided a 0.2 sccm N_2 flow in the opposing direction, matching the flow to be provided by the KP2 during the analytical separation phase in the *iGC2*. Desorption was performed by applying a 10.5 W pulse to the integrated thin-film heater, which heated the PCF2 to 180 °C in 10 s, immediately followed by a 2.7 W pulse for 5 s, which maintained this temperature. This relatively modest heating rate was selected for superior control and uniformity, while reducing the likelihood of stress fractures in the device, even though sharper desorption peaks are achievable with higher power.

Typical values of the resulting peak widths measured at half height (PWHH) were 3.2 s, 4.6 s, and 6.3 s for benzene, toluene, and *m*-xylene, respectively (figure 6(*b*)). Only minimal tailing was observed. Full desorption was achieved during the first thermal pulse, as verified by a second thermal pulse that did not provide any additional desorption peak.

The preconcentration factors were calculated by the volume ratios of the vapor sample to the thermal desorption, i.e., the product of the sampling flow rate and the sampling time divided by the product of the desorption flow rate and the desorption PWHH [30]. As calculated from figure 6(*b*),

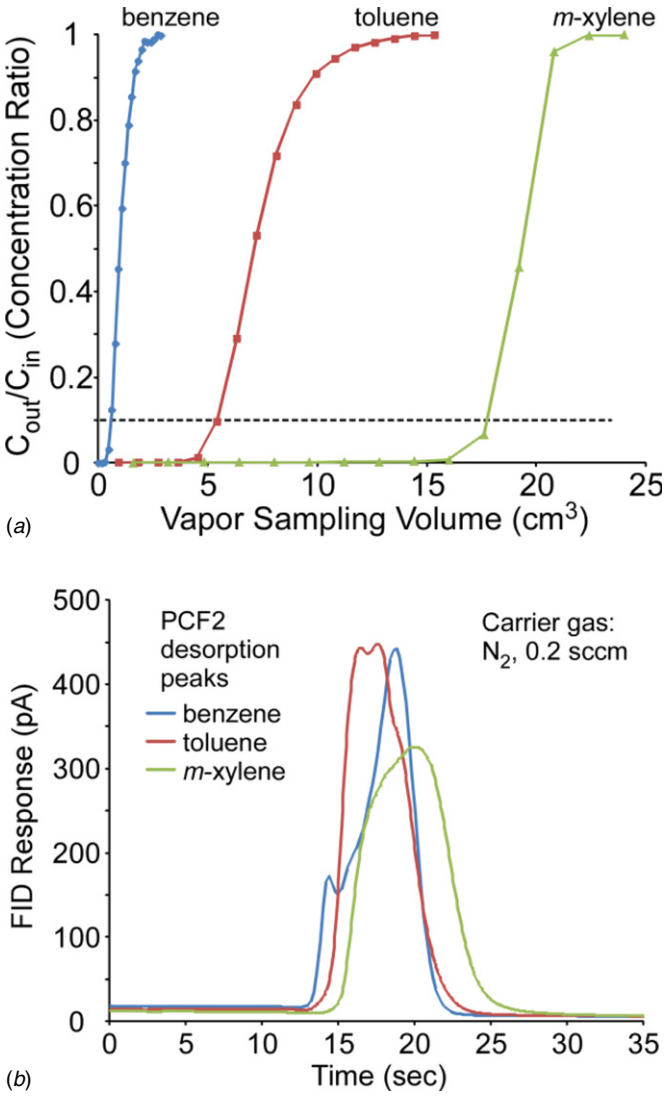

Figure 6. Evaluation of the performance of the PCF2. (*a*) The outlet BTX concentration response (normalized to the inlet concentration) during vapor sampling. (*b*) BTX desorption peaks with 0.2 sccm N_2 flow after sampling 1 cm^3 of vapor.

the preconcentration factors for toluene and *m*-xylene were 65 and 48, respectively. The value for benzene cannot be obtained from figure 6(*b*), because the 1 cm^3 sampling volume substantially exceeds its breakthrough volume (as illustrated in figure 6(*a*)). By sampling benzene and toluene with their breakthrough volumes, preconcentration factors of 25 and 236 were obtained. A preconcentration factor of 143 was obtained for *m*-xylene with a sampling volume of 3 cm^3. A thorough parametric sweep can identify the maximum preconcentration factors, but it is beyond the scope of this effort.

4.3. Column and detector

The separation columns were evaluated within an Agilent 6890 GC with a vapor injection port located upstream and an FID located downstream [8]. To provide a better demonstration of the separation capability of the column, the columns were used to separate BTX and five interfering alkanes (C_5–C_9) at room temperature, with N_2 carrier gas flowing at 0.2 sccm to mimic

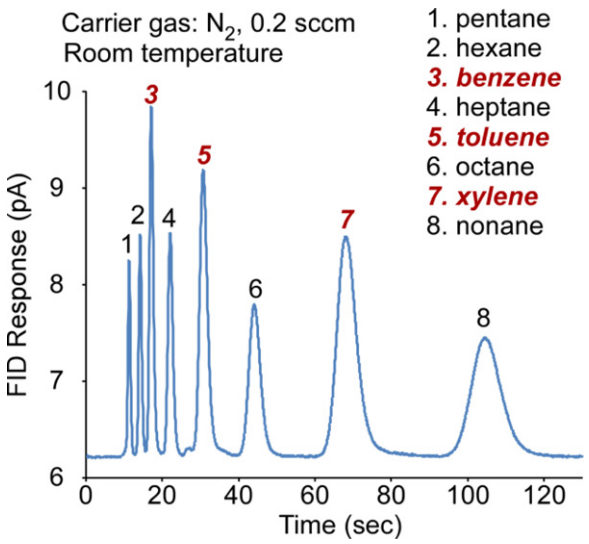

Figure 7. Typical separation of BTX and five alkanes provided by the column at room temperature. The injector and FID in an Agilent 6890 GC were used for testing the column.

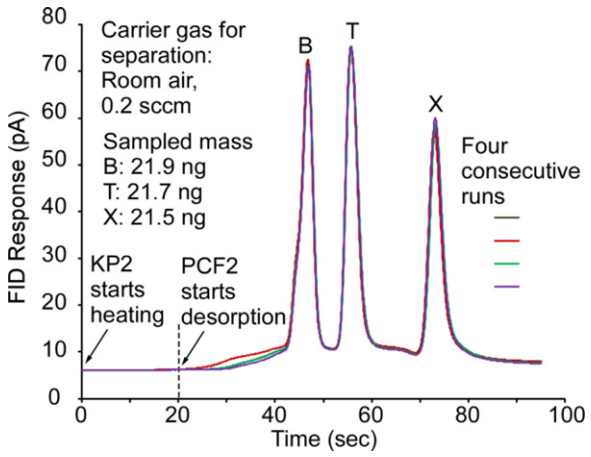

Figure 8. Four consecutive runs of BTX separations provided by a fully assembled *iGC2* system operated with a commercial FID. In each run, the system was used to analyze the same BTX vapor with the same sampling volume.

the KP2. The eight analytes were separated in less than 2 min (figure 7).

The discharge-based detector was operated with 3–5 ms voltage pulses of 800–1600 V. A handheld spectrometer (Model # USB 2000, Ocean Optics, FL) was used to monitor the optical emission [8]. As expected, the microdischarge showed strong optical emissions for N_2 within a wavelength range of 300–400 nm. The emission intensity at 388 nm, which is a characteristic line of C–H species, was used to quantify the BTX vapors eluting the column. To minimize the effect of pulse-to-pulse variation in emission intensity, the emission peaks at 388 nm were ratioed to the peaks for the N_2 line at 337 nm [28]. The detector was operated at 1 Hz (1 pulsed detection per second). With each microdischarge requiring ~10 mJ energy, the average power consumption was in the range of 10 mW, which was negligible compared to the power consumption of other *iGC2* components (i.e., the KP2 and PCF2). It is notable that such detectors can be operated at even lower energy levels [31].

4.4. The stacked iGC2 system

The fully assembled *iGC2* systems were tested in two different ways. In the first set of experiments, the discharge-based detector in the stacked system was not activated. Instead, the FID in an Agilent 6890 GC was used to evaluate the impact of the fluidic architecture upon the output. In the second set of experiments, the detector was utilized together with all other components, demonstrating the operation of the full system.

Vapor samples for these tests were prepared by evaporating liquid phase benzene, toluene, and *m*-xylene (each 0.1–2.7 μL) in a 2 L dilution bottle, resulting in vapor concentrations ranging from 43–1167 mg m^{-3}. The bottle and the *iGC2* system were previously purged using ultra-high-purity N_2 to minimize any impurities that might affect the evaluation of the system. With the bottle connected to End-B (figure 1) of the *iGC2* system, the KP2 was used to provide a sampling flow of 0.05 sccm for 5–15 min (using 3.3 W input power), drawing 0.25–0.75 cm^3 of the vapor through the detector and the column into the PCF2. Then the system was allowed to cool down naturally for ≈10 min.

In the first set of experiments, End-B (figure 1) of the *iGC2* system was then connected to the FID, whereas End-A remained open to ambient room air, which served as the carrier gas. The KP2 was then powered up to 1.3 W to provide 0.2 sccm air flow for 20 s before the PCF2 was powered up. This delay ensured a sufficient flow to be established prior to the analytical separation. The eluent from the column was identified and quantified by the FID. The tests were repeated four times in succession with each BTX vapor sample, using identical operating conditions in order to evaluate repeatability. Typical results are shown in figure 8; the repeatability is evident. As expected, the retention peaks of BTX appear as superposed onto a baseline response. The system operation parameters are summarized in table 1.

Continuing the first set of experiments performed with the FID detector, in order to demonstrate quantitative analysis, samples of BTX vapors were prepared with concentrations varying from 43–328 mg m^{-3}. Using the same *iGC2* parameters (table 1), the vapors were sampled at 0.05 sccm for 10 min, resulting a vapor sampling volume of 0.5 cm^3 and sampled masses of 22–164 ng. The FID chromatograms of the separations are shown in figure 9(*a*). To verify quantitative analysis, the areas of the retention peaks in the chromatograms (figure 9(*a*)) were calculated by subtracting from the peak response the underlying baseline area (figure 9(*b*)). The data points were fitted by straight lines connecting to the origin of the coordinate system, resulting in $R^2 \geqslant 0.9987$, which indicates good linearity of the system response for quantitative analysis.

In addition, sampling volumes were varied in the 0.25–0.75 cm^3 range (table 1). This was performed by varying the duration of the sampling period from 5–15 min. The resulting FID chromatograms and calculated peak areas are plotted in figures 10(*a*) and (*b*), respectively. In figure 10(*b*), the intercepts on the horizontal axis indicates the threshold

Table 1. Summary of the *iGC2* operation.

Component	Operation parameters		Figure
KP2	Sampling: 3.3 W, 0.05 sccm Separation: 1.3 W, 0.2 sccm		Figures 8–11
PCF2	Desorption: temperature ramped to 180 °C in 10 s using 10.5 W, and maintained for 5 s using 2.7 W		Figure 6(b) Figures 8–11
Column	Separation without active temperature programming		Figures 8–11
Discharge-based detector	Detection rate: 1 Hz; ~10 mW power		Figure 11
iGC2 system	Sampling time	BTX concentration	
	10 min	43 mg m^{-3}	Figure 8
	10 min	43–328 mg m^{-3}	Figure 9
	5–15 min	43 mg m^{-3}	Figure 10
	15 min	573–1167 mg m^{-3}	Figure 11

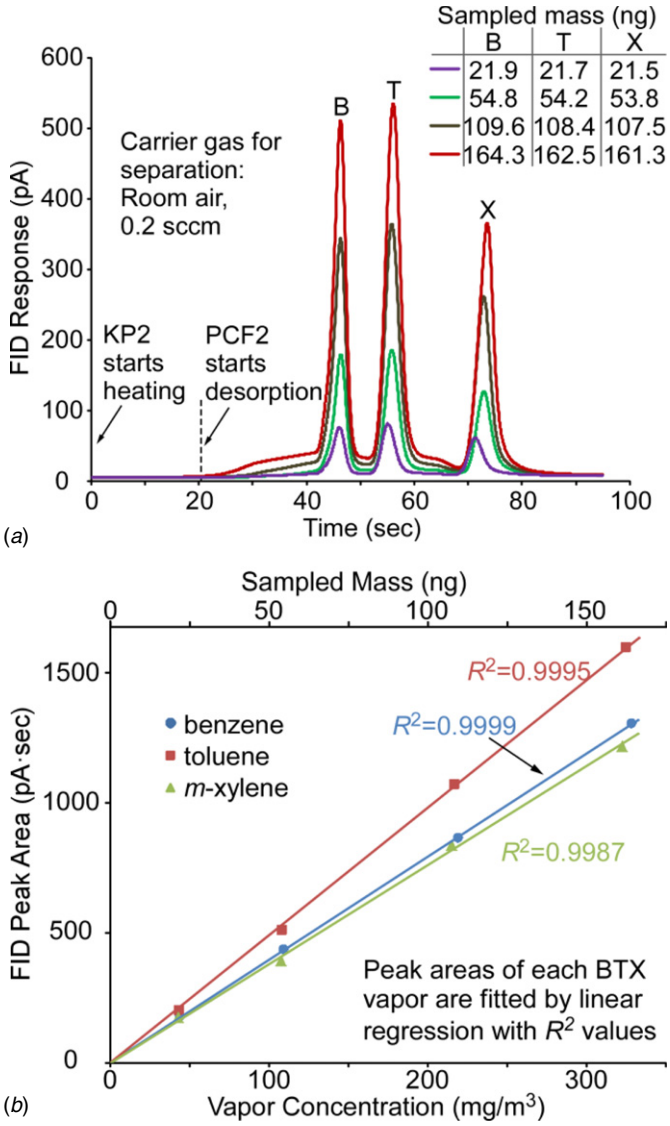

Figure 9. Quantitative separations provided by the *iGC2* system. (*a*) FID chromatograms of BTX vapors with the same sampling volume and various concentrations (and consequently various sampled mass). (*b*) Calculation of peak areas after subtraction of baseline areas, representing the analyzed masses.

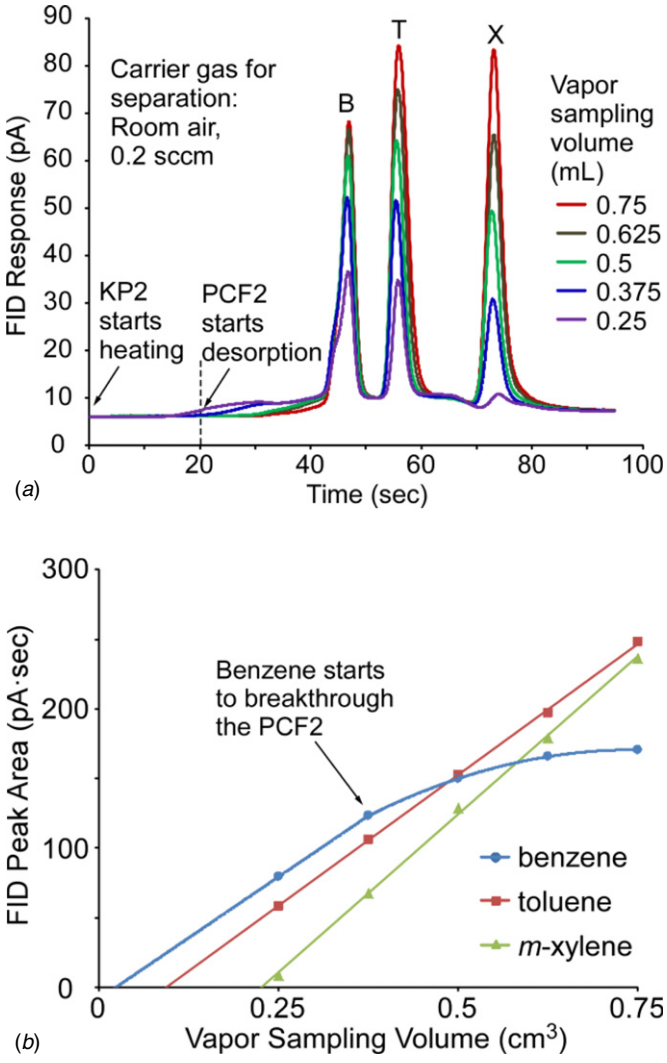

Figure 10. Characterization of the *iGC2* sampling operation. (*a*) FID chromatograms of the same BTX vapor with various sampling volumes. (*b*) Calculation of the peak areas. The intercepts on the horizontal axis indicate the threshold volumes (i.e., the volumes taken by the vapors to pass through the column during sampling).

volumes, i.e., the product of sampling times and flow rate taken by the vapor to pass through the column and detector before reaching the PCF2. As configured, the *iGC2* had threshold volumes of 0.02, 0.1, and 0.23 cm^3 for BTX, respectively. The sampling of benzene started to saturate when the sampling volume exceeded 0.4 cm^3, corresponding to the breakthrough of benzene in the PCF2.

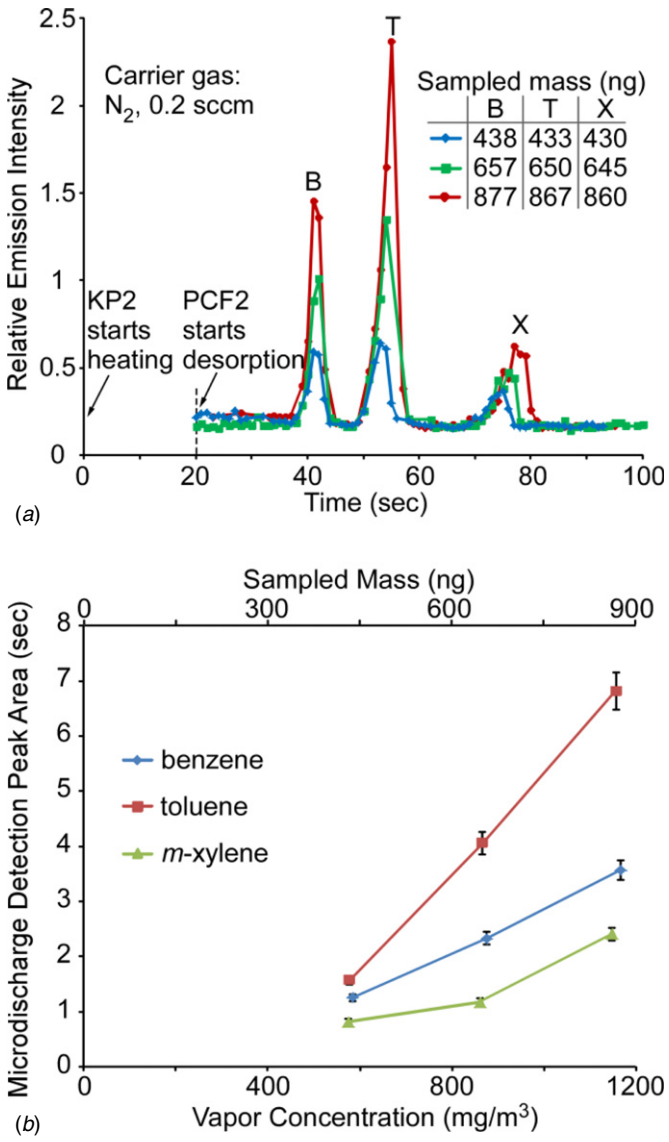

Figure 11. Full *iGC2* system operation with the use of the stack-integrated discharge-based detector. (*a*) Chromatograms of BTX vapors with the same sampling volume and various concentrations (and consequently various sampled mass). (*b*) Calculation of peak areas after subtraction of baseline areas, representing the analyzed masses.

In the second set of experiments conducted with fully assembled *iGC2* systems, the sampling procedure remained the same as the first set, as did the operating parameters (table 1). Samples of BTX with concentrations of 573–1167 mg m^{-3} were analyzed. To reduce the noise from spectral emissions of air, N_2 was used as the carrier gas by connecting a N_2-filled Tedlar® bag to End-A (figure 1) of the *iGC2* system. The resulting emission-intensity chromatograms (figure 11(*a*)) demonstrate separations of BTX with retention times similar to those shown in figures 8(*a*), 9(*a*), and 10(*a*). However, the peak heights of *m*-xylene are much smaller than those of toluene in figure 11(*a*). This is different from the FID chromatogram obtained with the same vapor sampling volume in figure 10(*a*), where toluene and *m*-xylene show similar peak heights. Additionally, the baseline fluctuations are not observed in figure 11(*a*). The calculated peak areas demonstrate positive correlations with sampled vapor concentrations, showing promise of quantitative analyses (figure 11(*b*)). However, in contrast to figure 9(*b*), the peak areas in figure 11(*b*) are not proportional to the vapor concentrations. This underscores the need for establishing the relationship between spectral intensity and vapor concentration for various analytes.

5. Discussion and conclusion

Overall, the experimental results validate the functionality of a valveless μGC architecture that utilizes a bi-directional micropump with a two-stage preconcentrator. Further, the results are repeatable, and quantitative analysis appears possible despite the modest flow rates provided by the motionless pump. The facile nature of the fabrication process holds promise for eventually developing a low-cost system. A number of observations can be made about the constitutive components and future work.

In contrast to a previously reported approach of using thermoelectric elements to implement a bi-directional Knudsen pump [25], the direct integration of heaters on both sides of the thermal transpiration membranes in the KP2 compromises flow rate in the sampling period (figure 5) for structural simplicity. Nevertheless, the small sampling flow rate can be compensated by extending the sampling period. In principle, bi-directional flow can also be achieved by using two opposing uni-directional pumps. In that case, however, each pump would be required to overcome the flow resistance of the other, which is less efficient than the use of a single bi-directional pump.

In the analytical separation periods, PCF2 provided 3–6 s-wide desorption peaks under the modest flow rate (≈0.2 sccm) available from KP2. Although the width of these desorption peaks may have contributed to the broadening of the retention peaks, quantitative analyses are evidently possible, as long as the retention peaks reach baseline-separation, i.e., a condition where the signal returns to the baseline between consecutive peaks (as demonstrated in figure 9). The dual-peak shapes of the benzene and toluene desorption in figure 6(*b*) are likely the result of the two stages within the PCF2 desorbing under a modest heating rate: the stage packed with Carbograph 2 desorbs slightly before the stage packed with Carbopack B.

It is notable that the relative heights of retention peaks measured by microdischarge-based detection (figure 11(*a*)) are different from those measured by the commercial FID (figure 10(*a*)). This is likely related to the difference between the two ionization methods that are involved. However, even with microdischarge-based detection, the calculated areas of the retention peaks are correlated to vapor concentration, demonstrating promise for quantitative analyses. This is encouraging, given the simple and unsealed nature of the microdischarge-based detector. The use of an N_2 carrier gas, and ambient contaminants can, however, increase the spectral noise [32, 33].

The overall system power consumption can be estimated from table 1. For a vapor sampling time of 10 min and separation duration of 1.5 min, the average system power

consumption is 3.2 W, which is dominated by the KP2 operation during the vapor sampling phase. This power consumption is higher than those of some of the previously reported systems (e.g., 0.7 W in [2], which uses a commercial pump), because of the inefficiency of the KP2 heat sink when driving flow during vapor sampling. Nevertheless, despite the relatively high power consumption, the Knudsen pump is still an attractive candidate for μGC integration, because of its compactness, simplicity in fabrication, and ultra-high reliability [24]. Thermal optimization of the system design and overall assembly are expected to reduce the power consumption.

A number of improvements can be envisioned for future designs of the *iGC2*. For example, a longer column can provide better separation of retention peaks, and heating of the column both during sampling and separation is likely to improve various aspects of the performance. In addition, the use of sorbents with higher surface area within the PCF2 would permit analyses of vapors with lower concentrations. All these approaches are intended to analyze more complex vapor mixtures. Nonetheless, a more powerful micro gas pump may be required to maintain the gas flow rate in a longer column. This can be accomplished by a multi-stage Knudsen pump. The stackable architecture in this work provides a simple and compact integration of the system, as well as the scalability to longer columns (by stacking multiple short columns). However, it is difficult for the stackable architecture to accommodate a multi-stage Knudsen pump, which requires more thermal isolation between multiple heaters and heat sinks. New architectures for multi-stage Knudsen pumps are currently under investigation.

The packaging of the system is still under investigation. One possibility is a case with an embedded heat sink, circuit board, and fittings for a mini-spectrometer. The lead transfer from the components to the circuit board could be accomplished by using pin assemblies.

Acknowledgments

The study was supported in part by the Microsystems Technology Office of the Defense Advanced Research Projects Agency High-Vacuum Program (DARPA Contract #W31P4Q-09-1-0011). Facilities used for this research included the Lurie Nanofabrication Facility (LNF) operated by the Solid-State Electronics Laboratory (SSEL) and the University of Michigan. The authors thank Professor Ken Wise and Mr Robert Gordenker for providing access to test facilities, and Dr Seungdo An for wafer metallization.

References

[1] Terry S C, Jerman J H and Angell J B 1979 A gas chromatographic air analyzer fabricated on a silicon wafer *IEEE Trans. Electron Devices* **26** 1880–6

[2] Gordenker R J M and Wise K D 2012 A programmable palm-size gas analyzer for use in micro autonomous systems *Proc. SPIE* **8373** 83731O

[3] Zampolli S, Elmi I, Mancarella F, Betti P, Dalcanale E, Cardinali G C and Severi M 2009 Real-time monitoring of sub-ppb concentrations of aromatic volatiles with a MEMS-enabled miniaturized gas-chromatograph *Sensors Actuators* B **141** 322–8

[4] Lewis P R *et al* 2006 Recent advancements in the gas-phase MicroChemLab *IEEE Sensors J.* **6** 784–95

[5] Manginell R P, Bauer J M, Moorman M W, Sanchez L J, Anderson J M, Whiting J J, Porter D A, Copic D and Achyuthan K E 2011 A monolithically-integrated μGC chemical sensor system *Sensors* **11** 6517–32

[6] Kim H, Steinecker W H, Reidy S, Lambertus G R, Astle A A, Najafi K, Zellers E T, Bernal L P, Washabaugh P D and Wise K D 2007 A micropump-driven high-speed MEMS gas chromatography system *IEEE Int. Conf. on Solid-State Sensors, Actuators and Microsystems Conf. (Transducers), (Lyon, France, June 2007)* pp 1505–8

[7] Liu J, Gupta N K, Wise K D, Gianchandani Y B and Fan X 2011 Demonstration of motionless Knudsen pump based micro-gas chromatography featuring micro-fabricated columns and on-column detectors *Lab Chip* **11** 3487–92

[8] Qin Y and Gianchandani Y B 2013 A facile, standardized fabrication approach and scalable architecture for a micro gas chromatography system with integrated pump *IEEE Int. Conf. on Solid-State Sensors, Actuators and Microsystems (Transducers), (Barcelona, Spain, June 2013)* pp 2755–8

[9] Adkins D R and Lewis P R 2009 Compact low-power gas detector for chemical alarms *SPIE Defense and Security Sensing Conf. Proc. (Orlando, FL)* 7304 73040S

[10] Lu C-J *et al* 2005 First-generation hybrid MEMS gas chromatograph *Lab Chip* **5** 1123–31

[11] Kim S K, Chang H and Zellers E T 2011 Microfabricated gas chromatograph for the selective determination of trichloroethylene vapor at sub-parts-per-billion concentrations in complex mixtures *Anal. Chem.* **83** 7198–206

[12] Collin W, Serrano G, Wright L K, Chang H, Nunovero N and Zellers E T 2013 Fieldable MEMS gas chromatograph for rapid determinations of explosive marker compounds in complex mixtures *IEEE Int. Conf. on Solid-State Sensors, Actuators and Microsystems (Transducers), (Barcelona, Spain, June 2013)* pp 2763–6

[13] Tian W-C, Chan H K L, Lu C-J, Pang S W and Zellers ET 2005 Multiple-stage microfabricated preconcentrator-focuser for micro gas chromatography system *J. Microelectromech. Syst.* **14** 498–507

[14] Oh K W and Ahn C H 2006 A review of microvalves *J. Micromech. Microeng.* **16** 13–39

[15] Robertson J K and Wise K D 1998 A low pressure micromachined flow modulator *Sensors Actuators* A **A71** 98–106

[16] Park J M, Evans A T, Rasmussen K, Brosten T R, Nellis G F, Klein S A and Gianchandani Y B 2009 A microvalve with integrated sensors and customizable normal state for low-temperature operation *J. Microelectromech. Syst.* **18** 868–77

[17] Henning A K *et al* 1998 Microfluidic MEMS for semiconductor processing *IEEE Trans. Compon. Packag. Manuf. Technol.* B **21** 329–37

[18] Potkay J A and Wise K D 2012 A hybrid thermopneumatic and electrostatic microvalve with integrated position sensing *Micromachines* **3** 379–95

[19] Qin Y and Gianchandani Y B 2014 A micro gas chromatograph with integrated bi-directional pump for quantitative analyses *IEEE Int. Conf. on Micro Electro Mechanical Systems (MEMS), (San Francisco, Jan. 2014)* pp 294–7

[20] Agah M, Potkay J A, Lambertus G, Sacks R and Wise K D 2005 High-performance temperature-programmed microfabricated gas chromatography columns *J. Microelectromech. Syst.* **14** 1039–50

[21] Narayanan S, Alfeeli B and Agah M 2012 Two-port static coated micro gas chromatography column with an embedded thermal conductivity detector *IEEE Sensors J.* **12** 1893–900
[22] Reynolds O 1879 On certain dimensional properties of matter in the gaseous state *Phil. Trans. R. Soc.* **170** 727–845
[23] Knudsen M 1909 Eine Revision der Gleichgewichtsbedingung der Gase. Thermische Molekularstromung *Ann. Phys. (Leipzig)* **336** 205–29 (in German)
[24] Gupta N K and Gianchandani Y B 2011 Thermal transpiration in mixed cellulose ester membranes: enabling miniature, motionless gas pumps *Microporous Mesoporous Mater.* **142** 535–41
[25] Pharas K and McNamara S 2010 Knudsen pump driven by a thermoelectric material *J. Micromech. Microeng.* **20** 1–7
[26] Seo J H, Kim S K, Zellers E T and Kurabayashi K 2012 Microfabricated passive vapor preconcentrator/injector designed for microscale gas chromatography *Lab Chip* **12** 717–24
[27] Barry E F 2004 Columns: packed and capillary; column selection in gas chromatography *Modern Practice of Gas Chromatography* ed R L Grob and E F Barry (New York: Wiley) pp 65–191
[28] Mitra B, Levey B and Gianchandani Y B 2008 Hybrid arc/glow microdischarges at atmospheric pressure and their use in portable systems for liquid and gas sensing *IEEE Trans. Plasma Sci.* **36** 1913–24
[29] Reidy S, Lambertus G, Reece J and Sacks R 2006 High-performance, static-coated silicon microfabricated columns for gas chromatography *Anal. Chem.* **78** 2623–30
[30] Namieśnik J 1988 Preconcentration of gaseous organic pollutants in the atmosphere *Talanta* **35** 567–87
[31] Mitra B and Gianchandani Y B 2008 The detection of chemical vapors in air using optical emission spectroscopy of pulsed microdischarges from two- and three- electrode microstructures *IEEE Sensors J.* **8** 1445–54
[32] Hoskinson A R, Hopwood J, Bostrom N W, Crank J A and Harrison C 2011 Low-power microwave-generated helium microplasma for molecular and atomic spectrometry *J. Anal. At. Spectrom.* **26** 1258–64
[33] Wilson C G, Gianchandani Y B, Arslanbekov R R, Kolobov V and Wendt A E 2003 Profiling and modeling of dc nitrogen microplasmas *J. Appl. Phys.* **94** 2845–51